

<sup>1</sup>Department of Earth and Planetary Sciences, McGill University, Montreal, QC, Canada

Keywords

Geo-spatial heat distribution, satellite image analysis, urban heat island, micro urban heat island

Email Correspondence

zoya.qudsi@mail.mcgill.ca

Sam Aucoin<sup>1</sup>, Alex Briand<sup>1</sup>, Béatrice Duval<sup>1</sup>, and Zoya Qudsi<sup>1</sup>

# Micro-Urban Heat Islands in the City of Montreal

## Abstract

Heat within a city is not evenly distributed, giving rise to regions of relatively warm and cold temperatures. Regions of very high heat are referred to as micro-urban heat islands (MUHIs) and can be severe enough to harm human health. Despite MUHIs being an important factor in urban health, they are extremely under-researched. In this study we mapped the locations of MUHIs on the island of Montréal and compared them with the locations of vegetation on three clear, sunny days: August 10th, 2021; July 6th, 2020; and June 20th, 2020 using Landsat 8 thermal images with 30 m resolution. We compared two criteria for MUHIs and quantified their composition based on unsupervised classification done on ENVI 5.6.1, and Normalized Difference Vegetation Index (NDVI) calculations. Our results show that MUHIs are mainly associated with the presence of asphalt and concrete, and the absence of dense vegetation. The presence of these materials is not, however, a strong predictor of the formation of MUHIs in themselves. Though variability in unsupervised classifications between images introduces uncertainty in MUHI composition, these results suggest that increasing dense vegetation coverage in Montréal could prevent MUHI development during the summer.

## Introduction

The micro-urban heat island (MUHI), or surface heat island, is a microclimatic phenomenon where isolated urban locations have high surface temperatures compared to surrounding areas<sup>1</sup>. There is no standard definition for what constitutes a MUHI; Aniello et al.<sup>1</sup> define a MUHI as any area whose surface temperature is higher than the maximum tree canopy surface temperature. Although MUHIs pose a serious risk to human health<sup>2-4</sup>, it is an extremely understudied phenomenon. This contrasts with general urban heat island (UHI) effect which is typically studied at a larger scale, such as an entire city having warmer surface and air temperatures than surrounding rural areas.

MUHIs are one of four main types of urban heat islands. While MUHIs are detected on micro-scales using remotely sensed land surface temperature (LST) data, an UHI may also be defined using air temperature and on local and meso-scales. Surface temperatures are often higher, and air temperatures are more sensitive to vegetation density. The two measures are, however, often closely linked<sup>5</sup>. Canopy and boundary layer heat islands are both defined based on atmospheric temperature differences between urban and rural areas; sub-surface heat islands are defined based on temperature differences between urban and rural subterranean ground. Despite the differences between the four types of UHIs, all arise from differences in the energy budgets between areas<sup>6</sup>.

Surface UHIs are associated with materials with a combination of [1] low albedo, which means less solar radiation is reflected and more is absorbed; [2] high heat capacity, which allows more energy to be stored; and [3] low emissivity, which is the effectiveness of a material in emitting energy, causing the surface temperature to be higher for a given amount of absorbed radiation<sup>7</sup>. Urban areas also have anthropogenic heat input from cars, electricity generation, and industrial processes which may contribute to the UHI effect<sup>8-10</sup>. The impact of anthropogenic heat on MUHIs has not been investigated. Additionally, heat distribution is profoundly affected by latent heat flux, which is the heat that is removed or added to a system via phase change processes like evaporation<sup>11,12</sup>. Vegetated areas lose significant amounts of latent heat via evapotranspiration. In the case of large green areas such as parks, this cooling effect extends outside of the area of the park<sup>13</sup>. For example, Jáuregui (1990)<sup>14</sup> found that the cooling effect of the Chapultepec Park, Mexico extends to a radius of 2 km around the park, which approximately corresponds to the width of the park. At smaller scales, vegetation can have a significant cooling effect through shading<sup>15,16</sup>. Besides the contributions of different materials to the urban landscape, the configuration of these materials, or surface form, is also important. To become surface heat islands, materials with the characteristics

listed must also be dry and be oriented to receive direct solar radiation<sup>17</sup>. The 3D structure of cities contributes to UHI formation by increasing the active surface area for energy exchange compared to flatter rural areas. Canyons formed by buildings and roads trap radiation through multiple reflection of incoming solar radiation between canyon walls and reduction of radiation loss from surfaces by shielding them from the cold sky. Canyons also shield urban surfaces from wind, which decreases sensible heat loss<sup>6</sup>. Though remote sensing can provide continuous LST data for an entire city, its images only provide a 2D overhead view. Therefore, it misses the contribution of vertical surfaces and structures which are critical to UHI phenomena<sup>18</sup>.

Previous work on MUHIs is mostly confined to the mapping of this phenomenon in different cities in the USA, Greece, and India<sup>1,19,20</sup>, and one study investigating their effect on heat-related mortality in Montréal<sup>2</sup>. MUHIs have not yet been mapped in Montréal nor have their mechanisms been studied despite this being an important aspect of the urban environment and health. Based on previous work, we expect that MUHIs in Montréal are located on urban surfaces such as asphalt and concrete, and that vegetation has a negative effect on MUHI formation.

The purpose of defining MUHIs is to understand the spatial distribution of urban heat. Materials within a city are distributed heterogeneously, meaning that some areas, such as parks and gardens, may radiate less heat than other areas such as parking lots or concrete buildings. Though MUHIs are defined based on surface temperature and not atmospheric temperature, which is what is experienced by pedestrians, hot urban surfaces still contribute to atmospheric heat islands and negatively impact human health. Understanding the spatial distribution will allow us to pinpoint urban locations that pose a larger risk to human health on very hot days and to identify which features exacerbate urban heating. Moreover, learning how MUHIs form can help predict future MUHI development and advise mitigation efforts.

## Methods

### Data Acquisition

We used Landsat 8 Collection 2 Level-2 images. Level-2 products, provided by the United States Geological Survey (USGS), are corrected for easy use and are freely available to the public. Landsat 8 images are collected at 30 meter resolution and at near-nadir angles ( $\pm 7.5^\circ$ )<sup>21</sup>. The images provided are already corrected by USGS for sensor degradation and changes, solar elevation, bandwidth, Earth-sun distance and effects of the atmosphere

to obtain surface reflectances<sup>22,23</sup>. These were then converted by USGS to land surface brightness temperatures using the Planck function<sup>24</sup>. Brightness temperature represents the temperature that a blackbody would have if it were emitting the same amount of radiation. Therefore, to calculate actual temperature, information on the emissivity of the ground must be known. The Level-2 products combine the Global Emissivity Database (GED), a measure global emissivity calculated through the Temperature–Emissivity Separation (TES) algorithm, and presented at 100-meter<sup>25</sup> resolution with brightness temperature<sup>26</sup>. The measurements for the GED are collected by a sensor on the Terra satellite, the Advanced Spaceborne Thermal Emission and Reflection Radiometer (ASTER), and values are accurate to  $\pm 0.015$ <sup>27</sup>, but can vary more in a city due to urban development and heterogeneity. The result is a land surface temperature product that is ready to use.

From Landsat’s collection of measured frequency bands, we used bands 1 to 5 and 10. Band 1 corresponds to ultra blue (443 nm), bands 2 to 4 to blue, green, and red (482 nm, 561.5 nm and 654.5 nm) respectively, band 5 corresponds to near infrared (NIR) (865 nm), and band 10 corresponds to thermal infrared (TIRS) (10895 nm)<sup>28</sup>. Combining bands 2 to 4 results in the visible true color image, and bands 4 and 5 are used to determine the Normalized Difference Vegetation Index (NDVI). We used bands 1-5 to classify surface cover types, and band 10 is used to obtain land surface temperatures.

In order to select comparable images, we used the Sentinel-Hub EO-Browser to visualise thermal images from Landsat 8. Three images corresponding to warm summer days with a clear sky within the last two years were qualitatively selected to have a comparable set of images in terms of meteorological conditions, urban development and overall surface temperature. These three images are from August 10<sup>th</sup> 2021, July 6<sup>th</sup> 2020, and June 20<sup>th</sup> 2020. All images are taken at a similar time of the day: from 10:30 to 11:30 AM EST. We downloaded the images from the USGS Earth Explorer platform.

#### Material Classification

**ENVI Classification** We performed a classification on all three selected images using ENVI version 5.6.1 to identify materials. The classifications were unsupervised, and classes were identified in post-processing. We used an Isodata (also known as Iso-cluster) unsupervised classification algorithm, consisting of a calculation of class means distributed across the image followed by an iterative clustering of remaining pixels using minimum distance. At each iteration, the mean is recalculated, followed by a reclassification of pixels according to this new mean<sup>29</sup>. We selected 2 combinations of bands for our classifications: bands 1 to 4 and bands 2 to 5. All images were layer-stacked as a combination of these selected bands and cropped in a quadrilateral over the region of Montréal. We entered a condition of 5 to 7 classes within the algorithm, with a total of 100 iterations for each classification.

Two classifications were performed on the August 10<sup>th</sup> image with bands 1 to 4 and 2 to 5 combinations. The classification for bands 1 to 4 has a total of 6 material classes, with 2 different classes corresponding to urban materials: one for asphalt and gravel, and a second one for concrete and rooftops. Vegetation for this classification is spread across 3 material classes: grass, grass and urban vegetation, and forest cover. Water is the final class. For bands 2 to 5, a total of 6 material classes are identified: urban materials (concrete and asphalt), concrete and highly reflective roofs, water, short vegetation (grass and urban trees), and forest cover. While some material classes, such as concrete and reflective roofs, appear on both classifications of the different multispectral images, the spatial distribution and accuracy of differentiating materials from one class to another may vary widely, meaning that despite having similar classes, both classifications are different.

Classifications for all images were completed using bands 1 to 4 because they made a clearer distinction between urban material classes. These classifications, however, proved to be variable between different images and

conditions; the 2020 images had one more material class than the 2021 image, and varying degrees of importance between the urban materials. We ultimately conducted the following analyses using the material classification from August 10<sup>th</sup> 2021, as it was the most precise classification performed in terms of defining and isolating urban materials of different nature. Though ENVI was effective in distinguishing urban materials, we did not judge its vegetation classification as satisfactory.

**NDVI Classification** We used the NDVI as an alternative method to classify vegetation across Montréal. The NDVI is an indicator of vegetation proportion by measuring the difference in near-infrared (NIR) and red (R) values for surface reflectance captured by satellite sensors<sup>30,31</sup>, based off the fact that NIR is scattered by mesophyll leaf structure, while red is strongly absorbed by chlorophyll<sup>32</sup>:

$$NDVI = \frac{NIR (band 5) - R (band 4)}{NIR (band 5) + R (band 4)},$$

where each band’s Surface Reflectance pixel values (PV) are scaled as follows<sup>33</sup>:

$$Surface Reflectance = 0.0000275PV - 0.2.$$

We applied a scaling factor because the Landsat Collection 2 Level-2 surface reflectance data product is stored in 16-bit integer format with values ranging from 0 to 65535. The scaling factor simply converts the unsigned 16-bit integer to a float value representing surface reflectance in usable units.

NDVI values run from -1.0 to 1.0. Areas of sparse vegetation, which include grass and areas with isolated shrubs or trees, show moderate NDVI values (approximately 0.2 to 0.5) while high NDVI values (approximately 0.6 to 0.9) correspond to dense vegetation such as forests<sup>34</sup>.

#### Image Manipulation

**Identifying MUHIs** The Landsat 8 thermal images (band 10) we selected were processed and analysed using the Rasterio package in Python. First, the surface temperature rasters were masked using a shapefile defining the island of Montréal<sup>35</sup>. Similar to the surface reflectance data products, the masked rasters were then converted to surface temperature in Kelvin using the following scaling factor<sup>33</sup>:

$$Surface Temperature (K) = 0.00341802PV + 149.0,$$

where PV is the Surface Temperature value at a given pixel in a raw Landsat 8 Collection 2 Level-2 surface temperature image. After we obtained surface temperatures in Kelvin, two temperature thresholds were applied. The first is defined as “any urban areas radiating higher temperatures than the warmest temperatures associated with tree canopy,” as defined by Aniello et al.<sup>1</sup>. Therefore, any area with a surface temperature greater than the highest dense vegetation temperature, found using NDVI, was considered a MUHI. The second threshold is defined as the top 2% of temperature values which was chosen since it roughly corresponds to two standard deviations above the mean, and can therefore be considered significantly higher than the mean temperature. By identifying which pixel temperatures are greater than the threshold, we generated a mask, or binary image, that shows MUHI locations on the map of Montréal.

**Comparing MUHIs and Surface Types** Similarly, we generated masks showing the locations of asphalt and concrete on the island by identifying pixels whose RGB values match the colour corresponding to that material in the classification. Masks were also generated to locate regions of dense and sparse vegetation. To compare MUHI locations and surface material types, we generated a third map by “overlapping” the MUHI and material masks. A new raster was created from these two masks by assigning

each pixel a value corresponding to one of the following: MUHI, material, MUHI and material, or neither.

## Results

The Tables 1, 2 and 3 summarize the main parameters obtained for images from August 10<sup>th</sup>, 2021, July 6<sup>th</sup> 2020, and June 20<sup>th</sup>, 2020, respectively, and compare the two temperature thresholds. In each, “Portion of a Material that Contains a MUHI” refers to the proportion of total area of each material on the island that is classified as a MUHI, and similarly, “Portion of MUHIs that Contain Material”, refers to the proportion of total MUHI area that is classified as that material. MUHIs are composed of mostly asphalt and concrete: more than 83%, 88% and 86% of MUHIs using either threshold definition are associated with one of these materials on August 10<sup>th</sup> 2021, July 6<sup>th</sup> 2020 and June 10<sup>th</sup> 2020 respectively. However, most asphalt and concrete are not part of MUHIs: on August 10<sup>th</sup> 2021, only 13.5% of asphalt-covered areas (unvegetated and vegetated) and only 8.83% of concrete-covered areas are associated with MUHIs defined by the 2% threshold, and even less for the canopy threshold. Results are similar for the 2020 images.

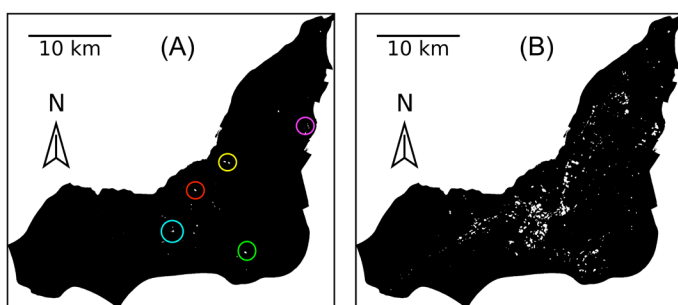


**Figure 1.** MUHI Distribution on the Island of Montréal on August 10<sup>th</sup> 2021. (A) Canopy threshold, (B) Top 2% threshold. MUHIs are in white. Notable MUHI locations are circled in (A): Trudeau International Airport (light blue), Bombardier Aerospace Complex (red), STM Centre de transport Legendre (yellow), Canadian Forces Base (pink), and Carrefour Angrignon (green).

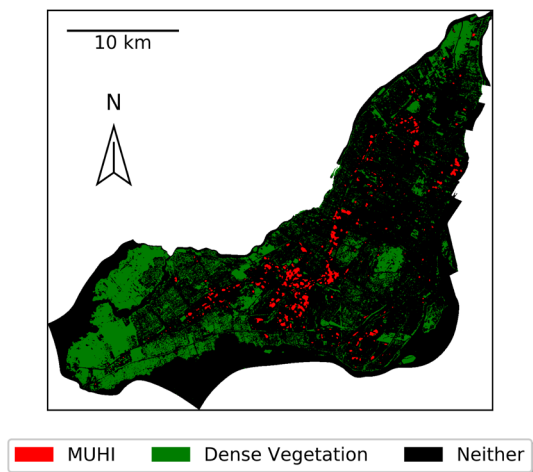


**Figure 2.** MUHI and Dense Vegetation Cover on the Island of Montréal on August 10<sup>th</sup> 2021. MUHIs have been identified using the top 2% threshold.

MUHI distributions for the tree canopy and the 2% thresholds were plotted over the island of Montréal for August 10<sup>th</sup> (see Fig. 1), 2021, July 6<sup>th</sup> 2020 (results not shown), and June 20<sup>th</sup>, 2020 (results not shown). MUHIs on the island are mainly located in Dorval and Saint-Laurent. These are where the Montréal Trudeau International Airport, the industrial Technoparc, and many large box stores are located.

To investigate the effects of vegetation on MUHI formation, we examined asphalt-covered areas that overlap with sparse vegetation and compare to asphalt areas with no vegetation. We found that unvegetated asphalt has

approximately 5-20 times more MUHI area than sparsely vegetated asphalt (Tables 1, 2 and 3). We also compared MUHI locations and dense vegetation coverage, shown in Fig. 2.

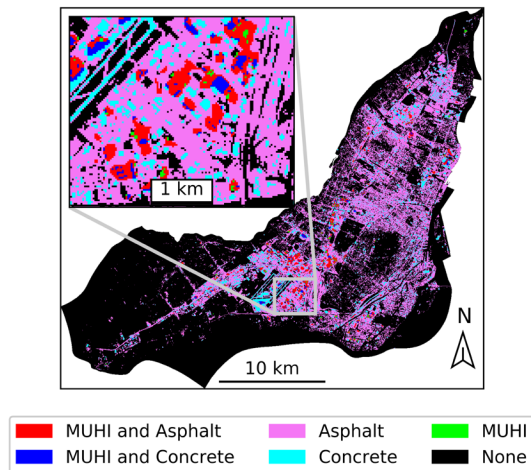


**Figure 3.** MUHI overlap with asphalt and concrete on August 10<sup>th</sup>, 2021. MUHIs are identified using the top 2% threshold. The region of the Montréal Trudeau International Airport is zoomed in.

**Table 1.** MUHI parameters for the two threshold definitions on August 10<sup>th</sup>, 2021.

August 10, 2021				
	Canopy Threshold		Top 2% Threshold	
Threshold Temperature	323 K		320 K	
Total MUHI Area	0.54270 km <sup>2</sup>		12.3237 km <sup>2</sup>	
	Portion of a Material That Contains a MUHI	Portion of MUHIs That Contains Material	Portion of a Material That Contains a MUHI	Portion of MUHIs That Contains Material
Concrete	0.74 %	40.43 %	8.83 %	21.13 %
Unvegetated Asphalt	0.40 %	38.94 %	11.21 %	47.14 %
Vegetated Asphalt	0.02 %	3.83 %	2.29 %	21.87 %
Sparse Vegetation	0.03 %	9.82 %	0.55 %	8.34 %
Dense Vegetation	0.00 %	0.00 %	0.02 %	0.18 %

**Table 2.** MUHI parameters for the two threshold definitions on July 6<sup>th</sup>, 2020.

July 6, 2020				
	Canopy Threshold		Top 2% Threshold	
Threshold Temperature	324 K		322 K	
Total MUHI Area	3.3246 km <sup>2</sup>		12.3534 km <sup>2</sup>	
	Portion of a Material That Contains a MUHI	Portion of MUHIs That Contains Material	Portion of a Material That Contains a MUHI	Portion of MUHIs That Contains Material
Concrete	2.91 %	25.85 %	8.41 %	20.07 %
Unvegetated Asphalt	2.51 %	56.06 %	9.62 %	57.77 %
Vegetated Asphalt	0.23 %	6.74 %	1.75 %	13.50 %
Sparse Vegetation	0.10 %	5.14 %	0.38 %	5.41 %
Dense Vegetation	0.00 %	0.00 %	0.01 %	0.09 %

**Table 3.** MUHI parameters for the two threshold definitions on June 20<sup>th</sup>, 2020.

June 20, 2020				
	Canopy Threshold		Top 2% Threshold	
Threshold Temperature	329 K		326 K	
Total MUHI Area	1.1079 km <sup>2</sup>		12.3543 km <sup>2</sup>	
	Portion of a Material That Contains a MUHI	Portion of MUHIs That Contains Material	Portion of a Material That Contains a MUHI	Portion of MUHIs That Contains Material
Concrete	1.32 %	35.09 %	7.79 %	18.59 %
Unvegetated Asphalt	0.67 %	46.95 %	8.99 %	56.42 %
Vegetated Asphalt	0.05 %	4.55 %	1.76 %	13.20 %
Sparse Vegetation	0.03 %	5.85 %	0.55 %	8.39 %
Dense Vegetation	0.00 %	0.00 %	0.02 %	0.14 %

## Discussion

### MUHIs and Surface Types

**Urban Materials** Areas with high MUHI density are sparsely vegetated and are dominated by asphalt and concrete surface coverage - all of these factors are known to enhance urban heating<sup>36</sup>. However, the presence of asphalt or concrete in itself does not necessarily lead to MUHI formation. In Montréal, most asphalt and concrete areas appear to lack other qualities that would otherwise make them MUHIs, namely receiving direct solar radiation. Because the measured quantity is surface temperature, a full picture of the effect of MUHIs is obscured since air temperature is more akin to what one would “feel”. Because of this, the intensity of MUHIs may be underestimated, and the effect of vegetation density maybe be underrepresented. In the absence of high-resolution air temperature measurements, remote sensing is the only way to study this phenomenon, despite it introducing a bias toward warmer temperatures. The images being taken early in the day also affects MUHI composition; urban materials with high heat capacities may be underrepresented as they did not have time to heat up, while materials with low heat capacities are overrepresented. Despite most asphalt and concrete not being part of MUHIs, MUHI composition is still dominated by these materials. This indicates that the surface material type influences MUHI generation, but is not the only factor.

**Vegetation** Our observation that unvegetated asphalt has several times more MUHI coverage than vegetated asphalt may be partly due to thermal anisotropy in cities, e.g. the satellite only detected the surface temperature of a tree and not the road beneath. Nonetheless, it is well-documented that vegetation can cool urban spaces through evapotranspiration<sup>37-39</sup>. The stark difference in MUHI coverage between vegetated and unvegetated asphalt suggests that vegetation plays some role in preventing MUHI development in Montréal. However, we found that sparse vegetation alone is not always sufficient to prevent MUHI formation; on August 10<sup>th</sup>, 2021, 9.82% of MUHIs as defined by the canopy threshold contained sparse vegetation.

Sparse vegetation includes grass, which dries out much faster during periods of low precipitation and becomes hotter. Soil moisture generally increases with depth<sup>40</sup>, so trees, which have deeper roots, have better access to moisture during dry spells and can continue transpiring to maintain cooler surface temperatures. Surface soil moisture varies diurnally and seasonally: high soil moisture is associated with cold near-surface air temperature and low near-surface wind speed, while dry soil is associated with warm temperatures and high wind speeds<sup>41</sup>. In Montréal, the monthly average precipitation in August 2021 was one of the lowest of that year (36.1 mm), while June and July 2020 had slightly more precipitation (46.4 and 86.8 mm, respectively)<sup>42</sup>. Low soil moisture may be

responsible for the greater contribution of sparse vegetation to MUHIs on August 10<sup>th</sup>, 2021 compared to the other two dates.

In our selected images, densely vegetated surfaces remained cooler overall. In addition to dense vegetation reducing heating on the surface where it is present, it may also reduce heating around the boundary of vegetation. In Fig. 2, we see that there is a MUHI-free buffer zone between the hottest areas (i.e., top 2% of surface temperatures) on the island and large areas of dense vegetation like Mount Royal Park and Morgan Arboretum. This buffering phenomenon has previously been observed for air temperatures<sup>13</sup>.

**MUHI Locations** As shown in Fig. 1, MUHIs as defined by the canopy threshold are sparsely distributed compared to the percent threshold - the former method is much more selective, as the canopy threshold temperature is much higher than the 2% threshold temperature (see Table 1). The highly selective canopy method allows the identification of specific locations and structures that are associated with the absolute hottest MUHIs on the island. Notable MUHI locations include the Montréal Trudeau International Airport (Dorval), the Canadian Forces Base of Montreal, the Bombardier Aerospace complex (Saint-Laurent), the STM Centre de transport Legendre, and the Carrefour Angrignon (LaSalle). In Fig. 3 we can see that these areas are not fully covered by MUHIs, but MUHIs are located towards the center of these areas. This is consistent with the observation in previous work that MUHIs are hottest at the center<sup>1</sup>. We consistently observe that urban locations surrounded by large, uninterrupted areas of urban surface cover, rather than vegetation, are most susceptible to MUHI formation.

## Limitations

**Material Classification** We found inconsistencies between the classifications with bands 1 to 4 of our 3 images, which introduces uncertainty in the MUHI compositions presented in Tables 1, 2 and 3. The unsupervised classification algorithm from ENVI version 5.6.1 identified 7 classes for both images from 2020, but identified 6 classes for August 10<sup>th</sup> 2021. Since the classification was unsupervised, clusters were identified automatically, which may introduce variability if the images were taken under different conditions. Vegetation cover and biomass, as well as vegetation species distribution can vary slightly in relatively short periods of time, which may introduce variability between classifications of images between 2020 to 2021. Knowing this, it is possible that the unsupervised classification algorithm generated different clusters between images from different periods, resulting in fewer material classes for the image in August 10<sup>th</sup> 2021. Moreover, the quadrilateral region of the images under which classifications were performed includes several fields and agricultural complexes. This likely introduced additional variability within the clustering done during the unsupervised classification. It is also important to note that the choice of bands introduced flaws within the unsupervised classification. The ultra-blue band (443 nm) easily penetrates water and vegetation, which often results in the classification of some vegetated areas as water and vice-versa<sup>44</sup>. However, classification from the combination of bands 1 to 4 proved to be more reliable to differentiate between urban materials than the combination of bands 2 to 5. It is possible that under different conditions, another combination of bands could have shown better results.

**Thermal Anisotropy** Another limitation is the effective thermal anisotropy, or uneven surface temperatures, produced by Montréal’s 3D geometry and uneven surface heating. This is particularly limiting in densely built areas like Montréal’s downtown core. Satellites only capture a 2D view of surface temperature, so some features may not be “seen” by the satellite. For example, a small park may be obstructed by a tall building; the satellite may only see the surface temperature of the building and mischaracterize the area as hotter than it actually is. Though Landsat 8 viewing angles are near-nadir, surface temperatures can still significantly vary between images collected at these slightly different angles. Vertical surfaces are almost entirely absent from the imagery, so we could not assess their contribution to MUHIs in Montréal.

## Conclusion

In this study, we identified the location and general causes of two definitions of micro-urban heat islands on the island of Montréal using 3 thermal images from the Landsat 8 Earth-observing satellite. Classifications done during our analysis identified several urban materials on the island of Montréal, but there were important factors that introduced variability within the unsupervised classification algorithm, thus affecting clustering and the number of classes between images. Using a larger set of images spread over a longer period of time could reduce variability. In addition, using a mask to isolate the island before classification could reduce the influence of agricultural activity in surrounding rural areas on the unsupervised classification clustering. Performing a supervised classification, while being more time consuming, could generate a much more reliable set of classified images. Areas of future work include analysing the seasonality and evolution of MUHIs using Landsat images over several seasons and years, and correcting for anisotropy by estimating Montréal's complete urban surface. This would include surfaces normally absent from satellite images, and thus provide a more accurate classification of materials and MUHIs on the island<sup>6</sup>.

In conclusion, we find that micro-urban heat islands on the island of Montréal are mainly associated with urban materials, but the presence of urban materials in itself is not a strong predictor for MUHI formation. We also find that almost no MUHIs (defined by the top 2% threshold) exist very close to dense vegetation; these zones act as a buffer to MUHI generation. In contrast to our hypothesis, we find that a significant proportion of MUHIs are associated with sparse vegetation, implying that not all forms of vegetation are equally efficient at reducing MUHI formation. These findings highlight the importance of dense green cover within Montréal to reduce the intensity of urban heating, and can be used to focus heat-related health mitigation efforts on the most vulnerable parts of the city, as well as inform building practices to reduce the generation and intensity of MUHIs.

## Acknowledgements

We thank Dr. Eric Galbraith, Dr. Jeff McKenzie, and Tanya Matitia for their support and comments throughout this project.

## References

1. Aniello, C., Morgan, K., Busbey, A. & Newland, L. Mapping micro-urban heat islands using LANDSAT TM and a GIS. *Computers & Geosciences* 21. Environmental Geology, 965–969. ISSN: 0098-3004. <https://www.sciencedirect.com/science/article/pii/0098300495000335> (1995).
2. Smargiassi, A. et al. Variation of daily warm season mortality as a function of micro-urban heat islands. *Journal of Epidemiology and Community Health* 63, 659–664 (2009).
3. Kovats, R. S. & Hajat, S. Heat Stress and Public Health: A Critical Review. *Annual Review of Public Health* 29, 41–55 (2007).
4. Hajat, S., O'Conner, M. & Kosatsky, T. Health effects of hot weather: from awareness of risk factors to effective health protection. *The Lancet* 375, 856–863 (2010).
5. Kawashima, S., Ishida, T., Minomura, M. & Miwa, T. Relations between surface temperature and air temperature on a local scale during winter nights. *Journal of Applied Meteorology and Climatology* 39, 1570–1579 (2000).
6. Oke, T. R., Mills, G., Christen, A. & Voogt, J. A. *Urban climates* (Cambridge University Press, 2017).
7. Goward, S. N. Thermal Behavior of Urban Landscapes and the Urban Heat Island. *Physical Geography* 2, 19–33. <https://doi.org/10.1080/02723646.1981.10642202> (1981).

8. Haddad, L. & Aouachria, Z. Impact of the transport on the urban heat island. *International Journal of Environmental and Ecological Engineering* 9, 968–973 (2015).
9. Ryu, Y.-H. & Baik, J.-J. Quantitative analysis of factors contributing to urban heat island intensity. *Journal of Applied Meteorology and Climatology* 51, 842–854 (2012).
10. Phelan, P. E. et al. Urban heat island: mechanisms, implications, and possible remedies. *Annual Review of Environment and Resources* 40, 285–307 (2015).
11. Holmer, B. & Eliasson, I. Urban-rural vapour pressure differences and their role in the development of urban heat islands. *International Journal of Climatology: A Journal of the Royal Meteorological Society* 19, 989–1009 (1999).
12. Liu, K., Li, X., Wang, S. & Li, Y. Investigating the impacts of driving factors on urban heat islands in southern China from 2003 to 2015. *Journal of Cleaner Production* 254, 120141 (2020).
13. Shashua-Bar, L. & Hoffman, M. E. Vegetation as a climatic component in the design of an urban street: An empirical model for predicting the cooling effect of urban green areas with trees. *Energy and buildings* 31, 221–235 (2000).
14. Jáuregui, E. Influence of a large urban park on temperature and convective precipitation in a tropical city. *Energy and buildings* 15, 457–463 (1990).
15. Sharlin, N. & Hoffman, M. The urban complex as a factor in the air-temperature pattern in a Mediterranean coastal region. *Energy Build.:(Switzerland)* 7 (1984).
16. Oke, T. R. The micrometeorology of the urban forest. *Philosophical Transactions of the Royal Society of London. B, Biological Sciences* 324, 335–349 (1989).
17. Oke, T. R. The energetic basis of the urban heat island. *Quarterly Journal of the Royal Meteorological Society* 108, 1–24 (1982).
18. Stewart, I. D. & Mills, G. *The Urban Heat Island* (Elsevier, 2021).
19. Stathopoulou, M., Cartalis, C. & Keramitsoglou, I. Mapping micro-urban heat islands using NOAA/AVHRR images and CORINE Land Cover: an application to coastal cities of Greece. *International Journal of Remote Sensing* 25, 2301–2316. <https://doi.org/10.1080/01431160310001618725> (2004).
20. Amirtham, L. R., Devadas, M. D. & Perumal, M. Mapping of Micro-Urban Heat Islands and Land Cover Changes: A Case in Chennai City, India. *The International Journal of Climate Change: Impacts and Responses* 1, 71–84 (2009).
21. Li, J., Roy, D. P. & Zhang, H. Comparison of Sentinel-2A and Landsat-8 Nadir BRDF Adjusted Reflectance (NBAR) over Southern Africa in AGU Fall Meeting Abstracts 2016 (2016), B31B–0472.
22. Thenkabail, P. S. Satellite Sensor Data Normalization Issues: A User Perspective <http://www.pancroma.com/downloads/General%20Landsat.pdf>. Oct. 2009.
23. United States Geological Survey. Landsat Collection 2 Level-2 Science Products <https://www.usgs.gov/core-science-systems/nli/landsat/landsat-collection-2-level-2-science-products> (2021).
24. Price, J. C. Estimating surface temperatures from satellite thermal infrared data—A simple formulation for the atmospheric effect. *Remote sensing of environment* 13, 353–361 (1983).
25. Hulley, G. C. et al. The ASTER Global Emissivity Dataset (ASTER

- GED): Mapping Earth's emissivity at 100 meter spatial scale. *Geophysical Research Letters* 42, 7966–7976 (2015).
26. United States Geological Survey. Landsat Collections [https://www.usgs.gov/core-science-systems/nli/landsat/landsat-collection-2-atmospheric-auxiliary-data?qt-science\\_support\\_page\\_related\\_con=1#qt-science\\_support\\_page\\_related\\_con](https://www.usgs.gov/core-science-systems/nli/landsat/landsat-collection-2-atmospheric-auxiliary-data?qt-science_support_page_related_con=1#qt-science_support_page_related_con).
  27. Sabol Jr, D. E., Gillespie, A. R., Abbott, E. & Yamada, G. Field validation of the ASTER temperature–emissivity separation algorithm. *Remote Sensing of Environment* 113, 2328–2344 (2009).
  28. Sentinel-Hub. About Landsat 8 OLI-TIRS Collection 2 Level 2 Data <https://docs.sentinel-hub.com/api/latest/data/landsat-8-l2/> (2021).
  29. Environmental Systems Research Institute. Fonctionnement de l'outil Iso cluster <https://desktop.arcgis.com/fr/arcmap/10.3/tools/spatial-analyst-toolbox/how-iso-cluster-works.htm>.
  30. Malik, M. S., Shukla, J. P. & Mishra, S. Relationship of LST, NDBI and NDVI using landsat-8 data in Kandai-himmat watershed, Hoshangabad, India (2019).
  31. United States Geological Survey. Landsat Normalized Difference Vegetation Index [https://www.usgs.gov/core-science-systems/nli/landsat/landsat-normalized-difference-vegetation-index?qt-science\\_support\\_page\\_related\\_con=0#qt-science\\_support\\_page\\_related\\_con](https://www.usgs.gov/core-science-systems/nli/landsat/landsat-normalized-difference-vegetation-index?qt-science_support_page_related_con=0#qt-science_support_page_related_con) (2021).
  32. Pettorelli, N. et al. Using the satellite-derived NDVI to assess ecological responses to environmental change. *Trends in ecology & evolution* 20, 503–510 (2005).
  33. United States Geological Survey. Landsat Collection 2 Level-2 Science Products <https://www.usgs.gov/core-science-systems/nli/landsat/landsat-collection-2-level-2-science-products> (2021).
  34. United States Geological Survey. NDVI, the Foundation for Remote Sensing Phenology [https://www.usgs.gov/core-science-systems/eros/phenology/science/ndvi-foundation-remote-sensing-phenology?qt-science\\_center\\_objects=0#qt-science\\_center\\_objects](https://www.usgs.gov/core-science-systems/eros/phenology/science/ndvi-foundation-remote-sensing-phenology?qt-science_center_objects=0#qt-science_center_objects) (2021).
  35. Ville de Montréal. Limite administrative de l'agglomération de Montréal (Arrondissements et Villes liées) 2020. <https://donnees.montreal.ca/ville-de-montreal/polygones-arrondissements> (2021).
  36. Kim, H. H. Urban heat island. *International Journal of Remote Sensing* 13, 2319–2336 (1992).
  37. Qiu, G.-y. et al. Effects of evapotranspiration on mitigation of urban temperature by vegetation and urban agriculture. *Journal of Integrative Agriculture* 12, 1307–1315 (2013).
  38. Qiu, G. Y. et al. Experimental studies on the effects of green space and evapotranspiration on urban heat island in a subtropical megacity in China. *Habitat international* 68, 30–42 (2017).
  39. Small, G., Jimenez, I., Salzl, M. & Shrestha, P. Urban heat island mitigation due to enhanced evapotranspiration in an urban garden in Saint Paul, Minnesota, USA. *WIT Transactions on Ecology and the Environment* 243, 39–45 (2020).
  40. Shi, B., Tang, C.-S., Gao, L., Liu, C. & Wang, B.-J. Observation and analysis of the urban heat island effect on soil in Nanjing, China. *Environmental Earth Sciences* 67, 215–229 (2012).
  41. Husain, S. Z., Bélair, S. & Leroyer, S. Influence of soil moisture on urban microclimate and surface-layer meteorology in Oklahoma City. *Journal of Applied Meteorology and Climatology* 53, 83–98 (2014).
  42. Total precipitation - monthly data for Montréal <https://montreal.weatherstats.ca/charts/precipitation-monthly.html>.
  43. Tigges, J., Lakes, T. & Hostert, P. Urban vegetation classification: Benefits of multitemporal RapidEye satellite data. *Remote Sensing of Environment* 136, 66–75 (2013).
  44. Acharya, T. D. & Yang, I. Exploring Landsat 8. *International Journal of IT, Engineering and Applied Sciences Research (IJIEASR)* 4, 4–10 (2015).